# Nanocatalysts Unravel the Selective State of Ag

Maximilian Lamoth,[a] Travis Jones,*[a] Milivoj Plodinec,[a] Albert Machoke,[b] Sabine Wrabetz,[a] Michael Krämer,[c] Andrey Karpov,[c] Frank Rosowski,[c, d] Simone Piccinin,[e] Robert Schlögl,[a, b] and Elias Frei*[a]

In the present work, we report on a comparative study of model catalysts during ethylene epoxidation reaction under industrially relevant conditions. The catalysts consist of Ag nanoparticles < 6 nm and a reference sample ~ 100 nm. Combining catalytic data with transmission electron microscopy, thermal desorption spectroscopy, and density functional theory allows us to show that catalytic performance is linked to the oxygen concentration in/on the Ag particles. Isotope experiments using $^{18}O_2$ and $C^{18}O_2$ are conducted to gain insight into the nature and location of oxygen in/on the Ag nanoparticles. The oxygen species responsible for the $CO_2$ formation and inhibition of the overall catalytic activity are identified, and the abundance of those species is shown to depend strongly on the pre-treatment and reaction conditions, showing both are critical for effective oxygen management. By comparison with a conventional Ag/$\alpha$-$Al_2O_3$ catalyst, we demonstrate a low concentration of oxygen in/on Ag leads to the highest selectivity regardless of particle size. However, particle size dependent oxophilicity leads to significantly lower TOFs for the Ag nanoparticles. This study provides fundamental understanding of the performance of supported Ag particles in ethylene epoxidation and offers new strategies to improve performance under industrially relevant conditions.

## Introduction

An intuitive approach to maximize the conversion of a catalyst is to increase its active surface area to provide more catalytically relevant reaction sites. This is accessible by, e.g., nanostructuring to increase the reactivity per unit mass relative to macroscopic crystals of the same substance.[1] Besides, the formation of nanoparticles of, typically, 1–10 nm gives rise to phenomena described as particle size (PS) effects.[2] This property has already been observed for a number of supported metal based catalysts like Co,[3] Ni,[4] Pd,[5] Pt,[6] Cu,[7] Ag[8] and Au.[9] The overall consensus from such observations is that the PS effect strongly depends on the kind of reaction as well as the active material, thereby leading to beneficial or detrimental effects.

The possibility of a PS effect for Ag in the partial oxidation of ethylene to ethylene epoxide (EO) has long captivated researchers, as it could act on EO selectivity and or conversion by altering the nature of the oxygen species on and in the Ag particles. Yet, after more than 40 years of research[10] it is still debated if a true Ag PS effect even exists, much less whether it contributes to EO selectivity and its role in oxygen management of real catalysts. An overview of some selected results dealing with the influence of the Ag particle size for supported Ag catalysts in the epoxidation of ethylene is shown in Scheme 1. Wu and Harriott[10b] studied supported Ag on silica in the range of 3–50 nm Ag PS and observed the highest conversions of ethylene, $X(C_2H_4)$, at around 5–6 nm, but with very low selectivity to ethylene epoxide, $S(EO)$, the latter steadily increased with increasing PS. Verykios et al.[11] investigated larger Ag particles, starting from 30 nm, and observed the same phenomenon for $S(EO)$, with a minimum in $X(C_2H_4)$ in the range of 50–70 nm Ag PS. This is in reasonable agreement with the observations of Wu and Harriot. However, since Verykios et al. normalized their rates per square meter of "free-metallic-silver surface area" determined by selective oxygen chemisorption, any comparison in terms of $X(C_2H_4)$ has to be interpreted with caution. Investigations of Cheng and Clearfield[12] showed a maximum of $S(EO)$ and $X(C_2H_4)$ at around 50 nm, with a

[a] Dr. M. Lamoth, Dr. T. Jones, Dr. M. Plodinec, Dr. S. Wrabetz, Prof. R. Schlögl, Dr. E. Frei
Fritz Haber Institute of the Max Planck Society
Department of Inorganic Chemistry
Faradayweg 4–6
14195 Berlin (Germany)
E-mail: efrei@fhi-berlin.mpg.de
        trjones@fhi-berlin.mpg.de
[b] Dr. A. Machoke, Prof. R. Schlögl
Max Planck Institute for Chemical Energy Conversion
Department Heterogeneous Reactions
Stiftstraße 34-36
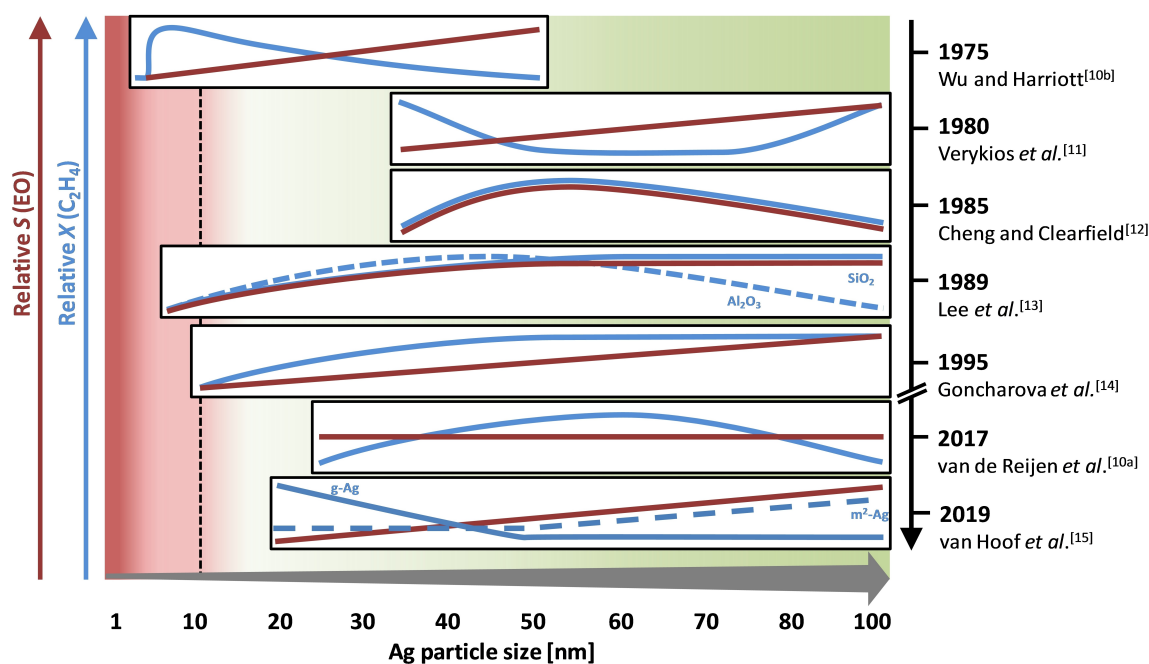45470 Mülheim an der Ruhr (Germany)
[c] Dr. M. Krämer, Dr. A. Karpov, Dr. F. Rosowski
Process Research and Chemical Engineering
Process Catalysis Research
BASF SE
67063 Ludwigshafen (Germany)
[d] Dr. F. Rosowski
BasCat-UniCat BASF Joint Lab
Technical University Berlin
Hardenbergstraße 36
10623 Berlin (Germany)
[e] Dr. S. Piccinin
Istituto Officina dei Materiali (CNR-IOM)
Area Science Park Basovizza
S.S. 14, Km. 163,5
34149 Trieste (Italy)

Supporting information for this article is available on the WWW under https://doi.org/10.1002/cctc.202000035

**ChemCatChem**

Full Papers
doi.org/10.1002/cctc.202000035

**Chemistry Europe**
European Chemical
Societies Publishing

**Scheme 1.** Overview of the catalytic activity of supported Ag catalysts in the epoxidation of ethylene. The reports are arranged regarding their investigated Ag particle size up to 100 nm schematically showing their conversion of ethylene $X(C_2H_4)$, their selectivity to ethylene epoxide $S(EO)$ and the year of appearance.

decrease in $S(EO)$ for larger PS in stark contrast to the aforementioned studies. Lee et al.[13] also observed a steady increase in $S(EO)$ for increasing PS, but this time from 6–50 nm and in the range of 50–100 nm $S(EO)$ remained unchanged. The $X(C_2H_4)$ showed a maximum at 40–50 nm in the case of corundum supported Ag and a plateau starting at around 60 nm for silica supported Ag. The Ag on corundum support performed similar to results reported by Cheng and Clearfield. Goncharova et al.[14] were able to show a steady increase in $S$ (EO) from 10–100 nm, which is in line with that reported by Wu/Harriot and Verykios et al., and a maximum in $X(C_2H_4)$ at around 50 nm in agreement with Cheng/Clearfield. The listed results were obtained during a period of 20 years and it took another 17 years until the group of Petra de Jongh investigated the PS of Ag and its influence on the ethylene epoxidation reaction. In contrast to the previous investigations, the $S(EO)$ at a constant low conversion of 2.8 % were compared, resulting in constant $S(EO)$ values. The achieved $X(C_2H_4)$ were again in agreement with previous studies, reaching its maximum at 60–70 nm. As a consequence, no PS effect on the selectivity in the range of 20–200 nm Ag PS was observed. A very recent study of van Hoof et al.[15] identified an increase in selectivity with PS (from ca. 20–200 nm). The *Ag weight*-based activity decreased until 50 nm and was stable afterwards. Besides, the *Ag surface area*-based activity was stable until 50 nm and increased with the Ag PS. The proposed explanation involves the complex interplay of Ag bulk, Ag crystallite size and grain boundaries, which remained rather elusive.

Since the synthesis of Ag particles < 10 nm is difficult to accomplish, only a limited number of studies are available.

Demidov and co-workers[16] investigating the model catalyst Ag/HOPG which stayed inactive for an average Ag PS of 8 nm. In contrast, 40 nm Ag particles on HOPG showed the formation of ethylene epoxide. These results stand contradictory to the report of Fotopoulus et al.,[17] where a catalyst with 9 nm Ag particles on MCM-41 showed a $X(C_2H_4)$ of up to 65 % with $S(EO)$ of 30–35 %. Such reasonable performances were comparable to the reference Ag/$\alpha$-Al$_2$O$_3$ catalyst with Ag particle sizes > 60 nm.

The essence of more than 40 years of research regarding the PS effect of Ag in the ethylene epoxidation reaction is unclear. The trends of the $S(EO)$ and $X(C_2H_4)$ curves illustrated in Figure 1 are arbitrary with respect to the Ag PS regimes. A maximum for $X(C_2H_4)$ for Ag PS around 50–60 nm, as well as a poor $S(EO)$ for small Ag particles seem to be consistent. But, the origin of the observed effects for different catalysts is still not clear and the observations often appear contradictory.

An explanation for the inconsistent situation in terms of a Ag PS effect might be the broad PS distributions achieved so far. Furthermore, the achieved Ag PS were above the relevant range, up to 6 nm, for which a dependence on catalytic performance is expected.[8,18] Besides, related oxidation reactions might also be helpful and serve as orientation for any PS effect. Lei et al.[8] used Ag cluster-based catalysts supported on silicon wafer in the range of 0.5–3.5 nm. Those small clusters and particles were active and selective in epoxidation of propylene with high turnover rates. Comparable results were achieved in our recently published study[19] of supported Ag catalysts in the oxidation of CO. *In-situ* synthesized Ag clusters < 1 nm showed exceptionally high CO oxidation rates com-
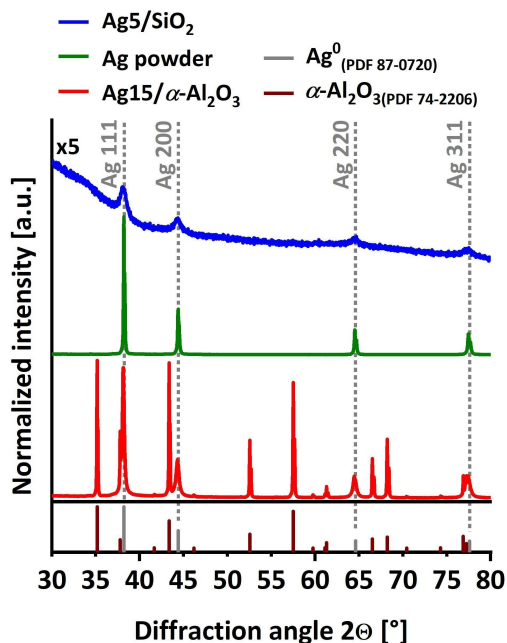
**Figure 1.** PXRD of Ag5/SiO$_2$ (blue, 5 times amplified), Ag powder as reference (green), Ag15/$\alpha$-Al$_2$O$_3$ (red) and the database entries for Ag$^0$ (grey, PDF 87-0720) and $\alpha$-Al$_2$O$_3$ (dark red, PDF 74-2206).

pared to Ag nanoparticles of 1–6 nm. Further, the Ag clusters and particles showed much higher CO oxidation rates than a Ag/$\alpha$-Al$_2$O$_3$ reference catalyst with 40 nm crystalline domain size.

Since both studies showed that Ag nanoparticles are able to perform oxidation reactions, the motivation of this study was to transfer these performances to the epoxidation of ethylene and to answer the long standing question of a Ag PS effect. Unraveling this possible PS effect is expected to lead to a deeper understanding of the selective state of Ag in general, as the PS effect has been linked to the nature of the adsorbed oxygen species present on active catalysts.[16]

Applying the recently introduced synthesis strategy,[19] SiO$_2$ supported Ag nanoparticles up to 6 nm with a narrow PS distribution are investigated. To ensure the relevance of the conducted study for any catalytic discussion, the samples are tested under industrially relevant conditions of high pressure. The performances of the Ag/SiO$_2$ catalysts are compared to a conventional Ag/$\alpha$-Al$_2$O$_3$ catalyst. All samples are thoroughly analyzed before and after catalytic testing by way of powder X-ray diffraction (PXRD) and transmission electron microscopy (TEM). Further, thermal desorption spectroscopy (TDS) allows us to identify the relevant Ag-O interactions related to the catalytic results. Within this study the adding of promoters on the catalyst or using organochloride as co-feed is excluded (as used on the industrially applied catalyst),[20] since it influences the origin of the Ag—O interaction and will be part of a separated manuscript.

## Experimental Section

### List of the used chemicals

Carl Roth, > 99.9%; Oxalic acid dehydrate: > 99%, Carl Roth; KOH: Merck, > 85%, for synthesis; Ethylenediamine: 99.5%; Fluka; $\alpha$-Al$_2$O$_3$: provided by BASF; Aerosil 300: Degussa; Ag powder: < 70 mesh, 99.999%, Alfa Aesar

**Synthesis of Ag/SiO$_2$ and Ag/$\alpha$-Al$_2$O$_3$** has already been described.[19] In short, a vacuum assisted impregnation technique was applied to achieve a controlled distribution on the support. For the silica (Aerosil® 300, Degussa, hydrophilic fumed silica powder, primary particles: spherical, 7–40 nm, no porosity) supported catalyst AgNO$_3$ was dissolved in water according to 5 wt.-% Ag loading (labeled as Ag5/SiO$_2$) and used as impregnation solution. The amount of H$_2$O needed for impregnation was determined by determining the "solvent capacity volume". The impregnated support was dried, transferred into 100–200 μm sieve fraction and subsequently calcined at 600°C for 1 h in a rotating tube furnace with a constant flow of 21% O$_2$ in Ar (300 ml·min$^{-1}$) with a heating rate of 2°C·min$^{-1}$.

For the synthesis of the industrial reference sample, 15 wt.-% Ag was loaded on $\alpha$-Al$_2$O$_3$ using an Ag oxalate based precursor according to patent literature, labeled as Ag15/$\alpha$-Al$_2$O$_3$.[20] The $\alpha$-Al$_2$O$_3$ support was then impregnated with the silver oxalate-ethylenediamine solution followed by a calcination under air.

**Ethylene epoxidation** was performed in a stainless steel plug flow reactor (inner diameter 4 mm) at 17.5 bar absolute pressure and a gas composition of 7/8/50/35 for O$_2$/Ar/N$_2$/C$_2$H$_4$ at a GHSV of 4850 h$^{-1}$. The temperature was raised stepwise with a 1°C·min$^{-1}$ heating rate and a dwell time of 6 hours for each temperature step. The composition of the exhaust gases was analysed online using a gas chromatograph (Agilent 7890 N) equipped with a FID and TCD detector. The samples were pre-treated for 24 hours at 210°C either in N$_2$ or synthetic air (named as O$_2$). For the kinetic analysis internal and external transport limitations, as well as heat transfer problems, are excluded by reference measurements (Figure S12).

**Ethylene oxide decomposition tests** were performed at 250°C under a constant flow of 1% EO in He. The temperature is higher than the actual testing temperature to force the EO decomposition. All tested samples were pre-treated in synthetic air at 250°C for 10 min. The Products were analysed by GC-MS analysis.

**Powder X-ray diffraction** (PXRD) patterns were recorded using a Bruker AXS D8 Advance II Theta/Theta diffractometer in Bragg-Brentano geometry using Ni filtered Cu K$_{\alpha1+2}$ radiation and a position sensitive LynxEye silicon strip detector. The sample powder was filled into the recess of a cup-shaped sample holder, the surface of the powder bed being flush with the sample holder edge (front loading). The resulting diffractograms were analyzed by full pattern fitting using the Topas software[21] to extract lattice parameters, crystallite sizes and Ag loading.

**Scanning transmission electron microscopy** (STEM) imaging was performed using a double Cs corrected JEM-ARM200CF (Jeol) operated at 200 kV and equipped with HAADF (high angle annular dark-field) and BF (bright-field) detectors. Samples were prepared by direct deposition of dry powder onto a Quantifoil Au holey grid. For the resulting histograms, the diameter of 1000 particles for Ag5/SiO$_2$ and 200 particles for Ag15/$\alpha$-Al$_2$O$_3$ were measured.

**Thermal desorption spectroscopy** (TDS) was applied for the temperature programmed desorption of oxygen. Therefore, a self-constructed setup which enables the testing of powder samples was used. The setup is equipped with mass flow controllers, an IR-

light furnace (BEHR IRF 10) and a mass spectrometer (PFEIFFER VACUUM QME 200). The powder sample is placed on a small quartz-glass boat which is placed in a quartz tube (inner diameter of 14 mm, outer diameter of 20 mm, length of 450 mm) located inside the furnace and connected to the system using Ultra Torr vacuum fittings. Prior to the desorption experiment the samples were pre-treated at 1 bar in 25% $O_2$ in Ar (synthetic air) at a flow of 100 ml·min$^{-1}$ for 12 h at 210°C, which cleans the surface of the sample and saturates the Ag with oxygen (surface and bulk). The gases are detected using the mass spectrometer leak valve. Afterwards the system is stepwise brought to $9 \cdot 10^{-7}$ mbar and directly connected to the mass spectrometer. The desorption experiment is conducted at a heating rate of 25°C·min$^{-1}$ up to 700°C. All masses and the temperature are monitored online.

**Inductive coupled plasma – optical emission spectroscopy (ICP-OES)** was used to determine the Ag loading of the catalysts. Therefore, the sample is solubilized using LiF, nitric acid and water at 230°C, diluted with water and analyzed with a PERKIN ELMER ICP OES Optima 8300.

**Microcalorimetry** was performed in a HT1000 (RT–1000°C) and MS70 (RT–100°C) Tian-Calvet calorimeter (SETARAM) combined with a custom-designed high vacuum (HV) and gas dosing apparatus. The sample was placed in batch reactor. $O_2$ and $C_2H_4$ adsorption experiments at 230°C were performed after cleaning the samples at 400°C for 15 h in $H_2$ (400 mbar). The reoxidation/regeneration at 350°C in $O_2$ was kept for 5 h (400 mbar).

**Density functional theory (DFT)** calculations were performed with the Quantum ESPRESSO package[22] at the PBE level including dispersion corrections with the exchange-hole dipole moment (XDM) model.[23] Following earlier work,[24] PAW datasets were taken from PS library[25] and used with a kinetic energy cutoff of 30 Ry. A k-point mesh equivalent to (12×12) for the (1×1) Ag(111) surface unit cell was employed along with Marzari-Vanderbilt smearing with a 0.02 Ry smearing parameter.[26] Minimum energy paths were computed with the climbing image nudged elastic band method using eight images for each path.

## Results and Discussion

The investigated catalysts consist of Ag particles on $SiO_2$ and $\alpha$-$Al_2O_3$. The low surface area $\alpha$-$Al_2O_3$ support serves as industrial reference with large Ag particles. To stabilize Ag nanoparticles in the range of ~2 nm a high surface area support material in the range of 300–400 m$^2$·g$^{-1}$ has to be used.[19] To avoid EO isomerization and combustion, support materials in the ethylene epoxidation reaction have to be chemically inert and with no acid functional groups. The used $SiO_2$ material fulfills the given criteria (Table 1, 328 m$^2$·g$^{-1}$) as thoroughly verified by EO decomposition experiments, conducted prior to the catalytic tests (Figure S1, Table S1). In the following the non-reducible supports are interpreted as inert without any further impact on the results.

### Sample preparation and characterization

According to an established synthesis protocol,[19] 5 wt.-% Ag supported on $SiO_2$ (Ag5/$SiO_2$) was prepared. In addition, a reference sample with 15.5 wt.-% Ag supported on $\alpha$-$Al_2O_3$

**Table 1.** Overview of the investigated catalysts with nominal and experimentally determined Ag loading (ICP-OES and PXRD), Ag domain size (PXRD full pattern fitting), support BET surface area (SA$_{BET}$) and internal number.

| Catalyst | Ag loading [wt.-%] (nom.) | (exp.) | Ag domain size [nm] | SA$_{BET}$ supports [m$^2$·g$^{-1}$] | FHI # |
|---|---|---|---|---|---|
| Ag5/$SiO_2$ | 5.0 | 4.4[a] | 6.5±0.7 | 328 | 29714 |
| Ag15/$\alpha$-$Al_2O_3$ | 15.5 | 12.4[a] 13.9[b] | 39.4±4.2 | 1.0 | 29934 |

[a] ICP-OES. [b] PXRD (Rietveld).

(Ag15/$\alpha$-$Al_2O_3$) was synthesized, following Rosendahl et al.[20] The corresponding PXRD are shown in Figure 1. The Ag15/$\alpha$-$Al_2O_3$ catalyst exhibits slightly broadened Ag reflections (in comparison to the Ag powder reference, Figure 1 green pattern) and reflections of $\alpha$-$Al_2O_3$. The widening is explained by the reduced domain size, which was determined to be 39.4±4.2 nm by full pattern fitting. Ag5/$SiO_2$ shows a pronounced broadening of the Ag reflections, a direct indication of the smaller domain sizes of 6.5±0.7 nm. The $SiO_2$ support is responsible for the diffuse reflection visible in the range of 30–40° 2Θ. The Ag lattice parameters are also determined for Ag5/$SiO_2$ and Ag15/$\alpha$-$Al_2O_3$ as 4.089±0.012 Å and 4.08603± 0.00009 Å, respectively. Within the uncertainty of the fitted results, the lattice parameters are in good agreement with the reported reference value of 4.086 Å[27] for Ag$^0$. Complementary to PXRD, STEM analysis was performed in order to extract the PS information illustrated in Figure 2. For Ag15/$\alpha$-$Al_2O_3$ the Ag particles are well distributed over the support (Figure 2a) with dominant PSs between 50–150 nm (see histogram inset Figure 2b, average PS 105 nm and a standard deviation of 86 nm) and a minor fraction of particles in the range of 20–40 nm and <200 nm. Figure 2b shows in addition the element specific EDX maps (see also Figure S2). The main PS determined by STEM are larger than the domain sizes determined by PXRD, indicating that the fraction of larger particles have been formed by sintering. The Ag particles were sometimes irregularly shaped (non-spherical), which explains the broad distribution. For Ag5/$SiO_2$ (Figure 2 c, d) the Ag particles are homogeneously distributed over the whole support with a very narrow size distribution (corresponding histogram inset Figure 2d, a PS of 2.3 nm and a standard deviation of 0.72 nm, see also Figure S3a). The absence of Ag particles larger than 5.8 nm is in good agreement with the results from PXRD (domain sizes of 6.5±0.7 nm). Since XRD is only sensitive to crystallites <2–3 nm, the main fraction of the Ag PS stays invisible and the XRD domain size is interpreted as upper limit. An overview of the relevant parameters of the used catalysts is presented in Table 1. The Ag loading was experimentally determined by ICP-OES and resulted in 4.4 wt.-% Ag for the Ag5/$SiO_2$ sample and 12.4 wt.-% for Ag15/$\alpha$-$Al_2O_3$. In addition, the quantitative PXRD analysis (Rietveld method) for Ag15/$\alpha$-$Al_2O_3$ determined the Ag loading to be 13.9 wt.-%. Generally, the quantitative assessments are in good agreement with the nominal values.

**ChemCatChem**

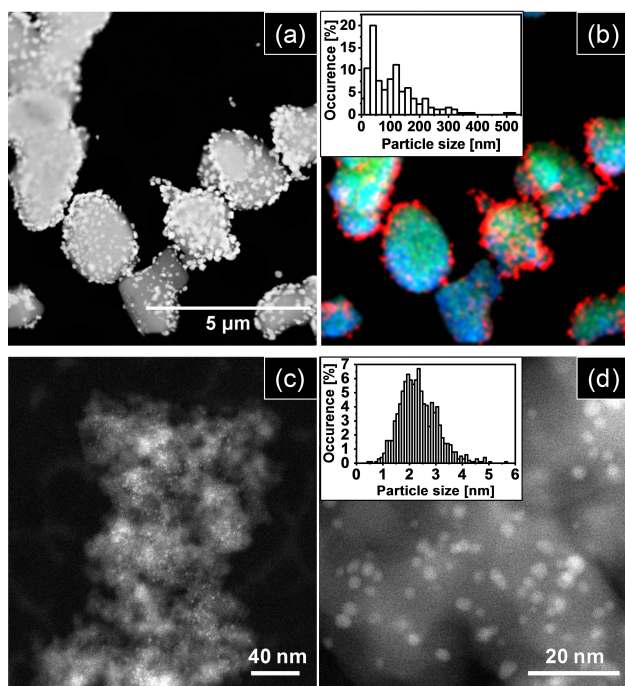**Full Papers**
doi.org/10.1002/cctc.202000035

**Chemistry Europe**
European Chemical
Societies Publishing

**Figure 2.** STEM ADF images of catalyst Ag15/$\alpha$-Al$_2$O$_3$ (A) and the corresponding elemental mappings of Ag red, Al green, O blue and particle size distribution (B, see also Figure S2 for EDX). STEM ADF of Ag5/SiO$_2$ (C). The bright spots refer to Ag particles. For catalyst Ag5/SiO$_2$ also the particle size distribution is shown (D).



**Figure 3.** Selectivity to ethylene epoxide as function oxygen conversion for catalyst Ag15/$\alpha$-Al$_2$O$_3$ (black triangle), Ag5/SiO$_2$–N$_2$ (blue squares) and Ag5/SiO$_2$–O$_2$ (green circles) at 17.5 bar, GHSV 4850 h$^{-1}$, C$_2$H$_4$:O$_2$ = 35:7.

## Ethylene epoxidation tests

All catalysts were tested in the epoxidation of ethylene to EO with applied gas feed, temperatures and pressures of the industrial process (without co-feeds, see also experimental part).[20] As a surface purification step, a pre-treatment temperature of 210 °C was chosen, which corresponds to the decomposition temperature of both Ag$_2$CO$_3$ (175 °C–225 °C[28]) and Ag$_2$O (~200 °C[29]). In the following, the pre-treatment atmospheres, which were varied for the Ag5/SiO$_2$ sample from N$_2$ to O$_2$ (synthetic air), is part of the label, i.e. Ag5/SiO$_2$-N$_2$ or Ag5/SiO$_2$–O$_2$ (this is not necessary for the reference catalyst since identical performances were obtained). Figure 3 shows $S$(EO) as a function of the oxygen conversion, $X$(O$_2$), at various temperatures (dwelled for 6 h each) for the Ag5/SiO$_2$–N$_2$, Ag5/SiO$_2$–O$_2$ catalyst and the Ag15/$\alpha$-Al$_2$O$_3$ reference. The performance of the Ag15/$\alpha$-Al$_2$O$_3$ catalyst in steady state follows a typical $S$ to $X$ behavior (lower selectivity at higher conversions) indicated by the grey line. Besides, the high selectivity towards EO is instantly reached and only at higher reaction temperatures (190 and 200 °C) an increase in $S$(EO) as function of time is observed (see also Figure S4, due to decreasing CO$_2$ rates). The Ag5/SiO$_2$–N$_2$ catalyst shows a pronounced activation period, for which the $S$(EO) steadily increases with time and temperature. The $S$(EO), e.g., increases from 48 % at 150 °C (after 2.5 h dwell time) to a maximum of 64 % at 180 °C, which is interpreted as successful activation. The corresponding $X$(O$_2$) shows only minor changes up to 180 °C (~4–7 %). Further
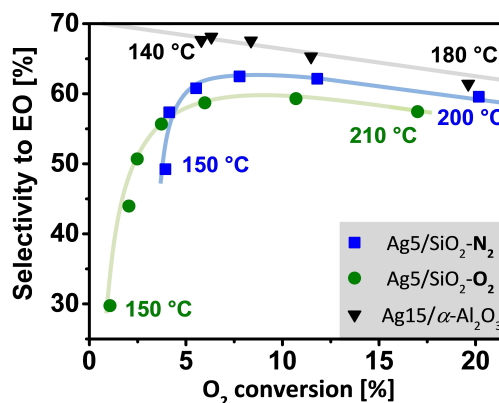
increasing the temperature leads to decreasing $S$(EO) and strong increase in $X$(O$_2$) following an expected $S$ to $X$ behavior. At ~210 °C Ag nanoparticles start to sinter and the Ag5/SiO$_2$–N$_2$ catalyst loses activity (see Figure S5, decrease of EO and CO$_2$ rates). Since the deactivation of the Ag5/SiO$_2$–N$_2$ catalyst starts already at 200 °C, the same catalyst was tested again until 230 °C (to trigger deactivation) and 180 °C (to avoid deactivation). The corresponding PS analysis (Figure S3c) after testing at elevated temperature shows a broad distribution of Ag particles until 40 nm (main PS ~ 5 nm). This serves as a textbook example of sintered particles continuously growing in size. In contrast, the PS distribution from the catalyst tested until 180 °C (highest $S$(EO)) remains narrow (Figure S3b, main PS ~ 2 nm, almost identical to the fresh sample S3a). The small increase of particles in the range of 1–2 nm is explained by the coalescence of Ag clusters still present after the calcination process.[19] Some of the Ag nanoparticles sintered, which is in line with the low Tammann temperature (< 100 °C ) of unsupported 2 nm Ag nanoparticles, however, since the sintering of the Ag nanoparticles lead to a loss in activity without influencing the $S$(EO) (Figure S5a 210 °C) the insignificant change of the PS distribution is excluded as source of the activation process.[30] This is supported by the loss in $S$(EO) at 230 °C (Figure S3c) demonstrating that sintering and $S$(EO) are decoupled phenomena.

Since we recently demonstrated that smaller Ag particles exhibit a stronger oxygen interaction,[19] it is reasonable to interpret the activation phase of the Ag5/SiO$_2$–N$_2$ catalyst as being influenced by its Ag–O chemistry. To gain further experimental evidence, the Ag5/SiO$_2$ catalyst was pre-treated in synthetic air (Ag5/SiO$_2$–O$_2$) before testing. We exclude sintering effects by synthetic air treatments since the catalyst was already calcined at 600 °C for 1 h. Figure 3 shows the direct comparison of Ag5/SiO$_2$–N$_2$ (blue) and Ag5/SiO$_2$–O$_2$ (green) catalysts. The Ag5/SiO$_2$–O$_2$ catalyst shows poor $S$(EO) and $X$(O$_2$) at low temperatures. In comparison to the Ag5/SiO$_2$–N$_2$ catalyst, its activation phase is more pronounced and prolonged. The completely activated state is not reached until 190 °C (maximum in $S$(EO) of 61 %) and generally the Ag5/SiO$_2$–O$_2$ catalyst

is less active (i.e. at 200 °C same $S$(EO) but only 50% of the conversion) than its Ag5/SiO$_2$–N$_2$ counterpart. However, upon increasing the temperature, the Ag5/SiO$_2$–O$_2$ catalyst still reaches the typical $S$-$X$ behavior (green line) seen for the other catalysts. In summary, the SiO$_2$ supported Ag nanoparticles show, after a distinct activation period, a promising catalytic performance in comparison to the Ag15/$\alpha$-Al$_2$O$_3$ reference. Since the increase in $S$(EO), and generally the different activation behavior of the catalysts, is not a sintering effect, the Ag–O interaction, respectively stored oxygen in/on Ag, might be responsible for the observed effects. This is supported by studies which show that the pre-treatment also pre-determines the existence of highly stable oxygen species in/on the Ag nanoparticles difficult to allocate for oxidation reactions.[12–13,31] The existence of highly temperature stable oxygen species for Ag nanoparticles below 6 nm[19] might also influence the catalytic performance and be responsible for the diverse picture of catalytic activities in oxidation reactions as illustrated in Scheme 1.

### Impact of the Ag-oxygen interaction

To have access to the oxygen concentration in/on Ag and the corresponding Ag-oxygen interaction, thermal desorption spectroscopy (O$_2$-TDS) was applied. A dedicated setup for powder samples was used, which allows a sample pretreatment under 1 bar and the subsequent desorption experiment at $10^{-6}$ mbar, as bridge between conventional TPD[32] (desorption in to inert gas) and surface science related TDS[33] experiments. The calcined catalysts were *in-situ* pretreated under Ar (Ag5/SiO$_2$–Ar 12 h at 210 °C, analogue to Ag5/SiO$_2$–N$_2$) or synthetic air (12 h at 210 °C) and compared to the Ag15/$\alpha$-Al$_2$O$_3$ reference, pre-treated under synthetic air as well (Figure 4a). The desorbed oxygen signal is normalized to the sample weight. For Ag5/SiO$_2$–O$_2$, two regions in which oxygen desorbs can be clearly distinguished, with region I (200 °C–500 °C) having a maximum at 350 °C and region II appearing for $T > 540$ °C (where Ag nanoparticles already start to melt). The temperature range for region I is consistent with the oxygen present in surface reconstructions on low miller index surfaces (e.g. nucleophilic oxygen) known to participate in combustion in model studies.[34] From desorption temperature alone, we cannot determine if the oxygen desorbing in region I is also associated with oxygen on the unreconstructed surface, a species that may participate in EO formation.[35] The desorption temperature for region II is in line with dissolved oxygen and/or electrophilic oxygen participating in EO formation during temperature programmed reaction.[24,36] However, since the mentioned oxygen species were identified on model systems, their roles and relevance for supported Ag catalysts remains rather speculative and will not be further discussed.

After pre-treatment in Ar the amount of O$_2$ desorption in region I is reduced by 54%. Region II, however, stays almost unaffected, emphasized by the converging amount of desorbed oxygen at around 620 °C. These different oxygen desorption signals indicate a critical correlation between the differences in
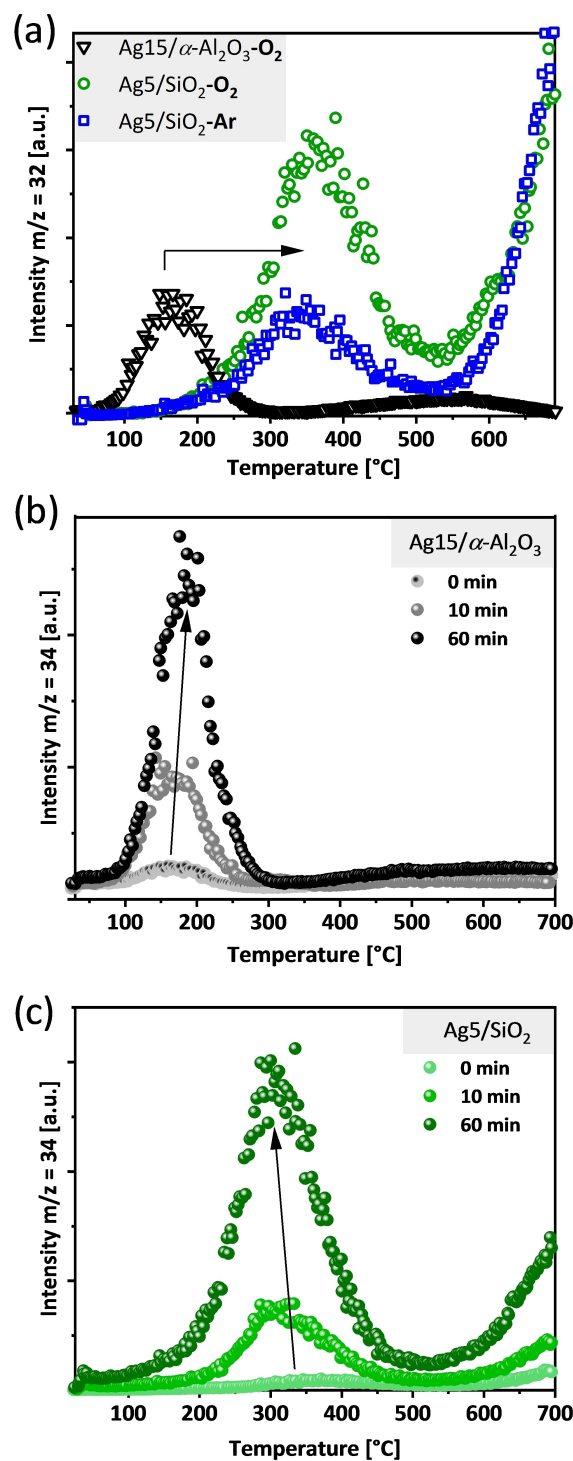


**Figure 4.** (a) O$_2$-TDS Ag5/SiO$_2$ pre-treated in Ar (blue), synthetic air (green) and Ag15/$\alpha$-Al$_2$O$_3$ in synthetic air normalized to the catalyst weight. (b) $^{18}$O$^{16}$O-TDS of Ag15/$\alpha$-Al$_2$O$_3$ treated for different times with $^{18}$O$_2$. (c) $^{18}$O$^{16}$O-TDS of Ag5/SiO$_2$ treated for different times with $^{18}$O$_2$.

activation behavior seen for the different pre-treatments, Ag5/SiO$_2$–N$_2$ and Ag5/SiO$_2$–O$_2$. The species desorbed in region I, with a high population on Ag5/SiO$_2$–O$_2$, likely reacts with ethylene to contribute to the unselective total oxidation reaction to CO$_2$ (see CO$_2$ formation rates Figure S5). Further, this

ChemCatChem

Full Papers
doi.org/10.1002/cctc.202000035

**Chemistry
Europe**
European Chemical
Societies Publishing

might be the origin of a possible blocking of the reaction sites and explain the lowered $X(O_2)$. The oxygen species desorbing in region II are not affected by the Ar pre-treatments, consistent with its assignment to dissolved oxygen.[24,36] The $O_2$ desorption behavior of the Ag15/$\alpha$-Al$_2$O$_3$–O$_2$ reference (pre-treated in synthetic air) is entirely different to the Ag5/SiO$_2$–O$_2$ sample. The temperature of the maximum in oxygen desorption is shifted by ~200°C to lower temperatures ($T_{max} = 165$°C) and a second desorption event is located a high temperatures (likely related to dissolved oxygen species). Besides, the quantity of desorbed oxygen is significantly decreased for Ag15/$\alpha$-Al$_2$O$_3$–O$_2$ (2.49 μmol(O)/g$_{cat}$) compared to Ag5/SiO$_2$–O$_2$ (14.64 μmol(O)/g$_{cat}$). Calculating the Ag:O ratio (based on the Ag loading of the samples) as indication for the oxygen concentration in/on Ag, the Ag nanoparticles are significantly enriched in oxygen by a factor of ~20 (Ag:O = 30 vs. 600 for Ag15/$\alpha$-Al$_2$O$_3$, only the first desorption events are integrated, for Ag5/SiO$_2$ range of ~200–500°C and for Ag15/$\alpha$-Al$_2$O$_3$ the range of ~100–300°C). Since the samples were pre-treated identically (saturated with oxygen at 210°C for 12 h) and the heating rates were also the same (25°C/min), a shift of the desorption temperature is interpreted as a change of the electronic structure of the Ag and the strength of the Ag–O interaction, respectively. This is similar to TPD studies on supported Au samples, which also identified a size dependent desorption energy excluding support effects.[37] However, based on the different quantities of the desorption (Ag:O ratios, as a consequence of the stronger Ag:O interaction and the high dispersion on SiO$_2$) and the shift in the $T_{max}$, the surface or subsurface location of the oxygen cannot be deduced. To aid in the assignment of the oxygen species observed in TDS, isotope exchange experiments with $^{18}O_2$ were conducted inside the TDS setup. After pre-treating the Ag15/$\alpha$-Al$_2$O$_3$ and Ag5/SiO$_2$ catalysts for 12 h at 210°C in synthetic air, the exposure times of $^{18}O_2$ was adjusted to 0 min, 10 min and 60 min (also at 210°C). Figure 4(b) and 4(c) show the desorption signal of m/z = 34 for Ag15/$\alpha$-Al$_2$O$_3$ and Ag5/SiO$_2$, which represents the mixed labeled oxygen isotopomer ($^{16}O^{18}O$). As a function of time, the mixed labeled oxygen increases (no change of m/z = 36, see also Figure S6), which implies that the oxygen (here: $^{18}O_2$) is dissociatively activated, accumulating as atomic oxygen in/on Ag. The recombination of stored ($^{16}O$) and exchanged ($^{18}O$) oxygen corresponds to a second order desorption kinetic,[33c] independent of the Ag particles size and desorption temperature. The shift of the $T_{max}$ with an increased saturation of labeled oxygen to higher (Ag15/$\alpha$-Al$_2$O$_3$, Figure 4b) and lower (Ag5/SiO$_2$, Figure 4c) temperatures represents attractive (higher $T$) and repulsive (lower $T$) interactions of the adsorbed species.[33b] This seems to be conclusive since the oxygen concentration in/on Ag5/SiO$_2$ is significantly higher. Besides, the labeled $^{18}O$ oxygen species are also desorbing in the high temperature regions as mixed labeled $^{16,18}O_2$, which are likely related to subsurface or dissolved oxygen species. Since the exchange of oxygen was conducted at 210°C, diffusion processes are very likely involved.

To elucidate the accessibility of the atomic oxygen species in/on Ag, a second experiment with C$^{18}O_2$ was conducted. Such a test can efficiently identify the surface atomic oxygen species

(all known forms of adsorbed atomic oxygen readily react with CO$_x$ to form surface carbonates), while dissolved and electrophilic oxygen has low propensity to form carbonates (Scheme 2).[38][39] To avoid the issue of carbonate formation and subsequent isotope mixing on the surface by contact to the environment, the precursor samples (e.g. AgNO$_3$/SiO$_2$) were first *in-situ* calcined in synthetic air. The *in-situ* generated Ag5/SiO$_2$–O$_2$ and Ag15/$\alpha$-Al$_2$O$_3$–O$_2$ catalysts were subsequently exposed to only C$^{18}O_2$ at 40°C for 30 min to saturate the surface.

While oxygen is able to migrate/diffuse into the TDS accessible sub-surface region of Ag during the *in-situ* generation step, the low temperature C$^{18}O_2$ exposure ensures the surface limited carbonate formation cannot access these buried species.[39b] The carbonates formed during C$^{18}O_2$ exposure are consequently partially labeled "Ag$_2$C$^{18}O_2$$^{16}O$". Temperature induced decomposition of the surface carbonates results in the release of CO$_2$, which is either mono- (C$^{18}O^{16}O$, m/z = 46) or double-labeled (C$^{18}O_2$, m/z = 48). If all the C$^{18}O_2$ adsorbs to form carbonate with pre-adsorbed $^{16}O$ the statistical ratio of C$^{18}O_2$:C$^{18}O^{16}O$ will be seen during TDS (e.g. 1:2 for tridentate or 1:1 for bidentate carbonate), however, since different types of carbonates might contribute a rather qualitative statement seems reliable.[33a] Conversely, if free surface is available or the oxygen is not accessible, C$^{18}O_2$ will adsorb and desorb as m/z = 48 in TDS.[40] The dominant desorption species for Ag5/SiO$_2$ (Figure 5b) is identified as C$^{18}O_2$ with a distinctly smaller desorption event for C$^{18}O^{16}O$ both appearing at a desorption temperature in the range of surface carbonates or weakly bound CO$_2$.[39b,40–41] The fraction of oxygen species able to interact with adsorbed C$^{18}O_2$ seems to be insignificant, also confirmed by reference measurements with pure C$^{18}O_2$. This means the stored oxygen in/on Ag, which forms under reaction conditions unselectively CO$_2$, is due to the strong Ag–O interaction of the nanoparticles unable to form carbonates. Saturating the surface of Ag15/$\alpha$-Al$_2$O$_3$ with C$^{18}O_2$ offers a different picture (Figure 5a). At low temperatures again C$^{18}O_2$ is mainly detected, but at elevated temperatures the amount of mixed labeled C$^{16,18}O_2$ increases significantly. This is a clear indication that oxygen stored in the Ag15/$\alpha$-Al$_2$O$_3$ sample is accessible and, at least in parts, located on the surface. The quantities of the desorbed CO$_2$ traces (m/z = 46 and 48) was nearly equal for both catalysts, which is line with our interpretation that the amount of oxygen stored in/on Ag5/SiO$_2$
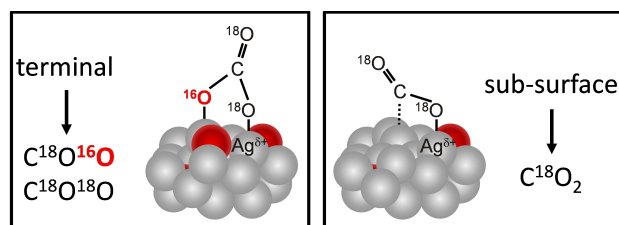
**Scheme 2.** Possible surface Ag$_2$CO$_3$ formation on Ag nanoparticles via terminal or sub-surface oxygen. In the case of sub-surface oxygen C$^{18}O_2$ might adsorb on the Ag surface and desorb also as C$^{18}O_2$.
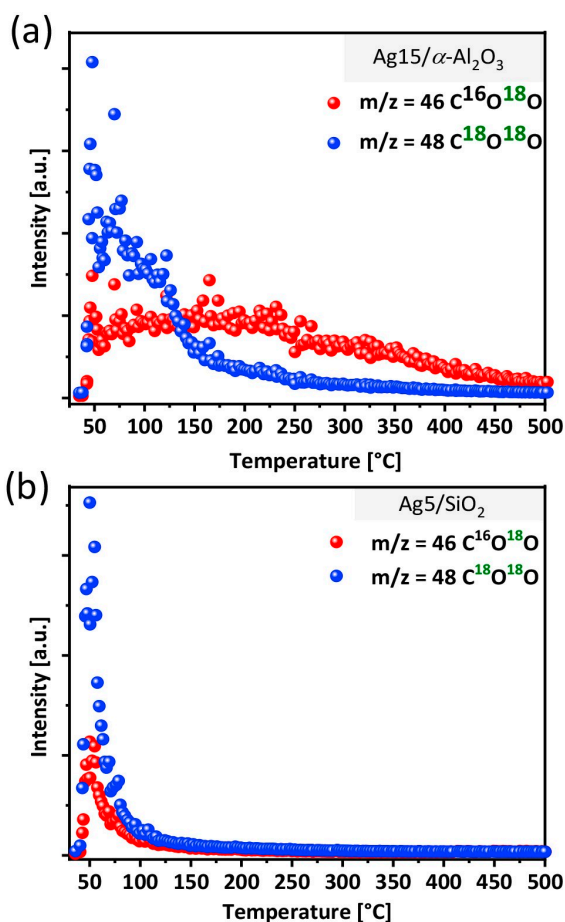
**ChemCatChem**

Full Papers
doi.org/10.1002/cctc.202000035

**Chemistry
Europe**
European Chemical
Societies Publishing

(a) Ag15/$\alpha$-Al$_2$O$_3$
- m/z = 46 C$^{16}$O$^{18}$O
- m/z = 48 C$^{18}$O$^{18}$O

(b) Ag5/SiO$_2$
- m/z = 46 C$^{16}$O$^{18}$O
- m/z = 48 C$^{18}$O$^{18}$O

**Figure 5.** *In-situ* calcined catalysts saturated with C$^{18}$O$_2$ at 40 °C. Heating rates of 25 °C/min were applied. CO$_2$ signals m/z = 46 (red circles) and 48 (blue circles) are shown for (a) Ag15/$\alpha$-Al$_2$O$_3$ and (b) Ag5/SiO$_2$.



Ag5/SiO$_2$
- Before EO
- After EO 1 bar
- After EO 17.5 bar

**Figure 6.** O$_2$-TDS for Ag5/SiO$_2$ pre-treated in synthetic air (green) with subsequent ethylene epoxidation at 230 °C at 1 bar (red). Additionally, the desorption spectrum of catalyst Ag5/SiO$_2$–N$_2$ after reaching steady state in ethylene epoxidation at 180 °C is shown (dark red).

is not accessible for carbonate formation under the selected conditions.

To test the necessity of stored oxygen in epoxidation, the influence of oxygen on the catalytic performance was further evaluated by TDS experiments simulating the activation period. The *in-situ* created Ag5/SiO$_2$–O$_2$ catalyst was tested at 1 bar and reaction feed (C$_2$H$_4$:O$_2$ = 5:1) for 4 h at 230 °C in the TDS setup (Figure S7a). After reaching a steady state conversion, the resulting O$_2$-TDS spectrum was recorded (Figure 6). A significantly reduced amount of oxygen desorbed from the catalyst in region I (green and red curves Figure 6). In addition, a completely activated Ag5/SiO$_2$ catalyst tested under 17.5 bar was transferred to the TDS setup and an oxygen desorption experiment was conducted. The corresponding O$_2$ desorption signal is negligible, demonstrating a correlation between the selective catalytic performance and the oxygen poor state. The same behavior is observed for the Ag15/$\alpha$-Al$_2$O$_3$ sample, after in-situ activation under reaction feed (Figure S7b + c and Figure S8). Generally, activating a supported Ag catalyst, independent of the respective particle size, leads in the TDS accessible range to an oxygen poor and selective catalyst. The consecutive removal of the oxygen species (at first completely in region I
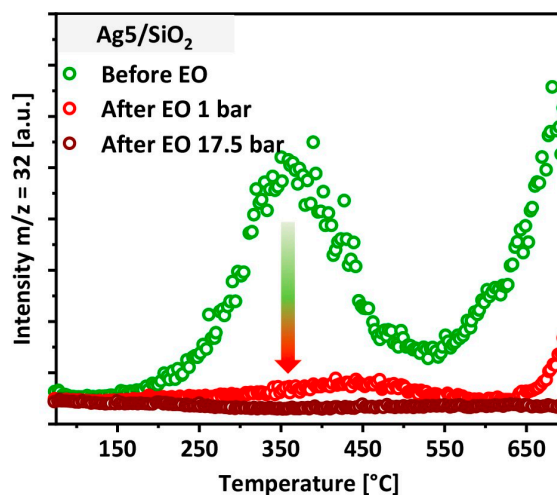
where nucleophilic oxygen, and afterwards incompletely in region II where dissolved and/or electrophilic oxygen might be located) is tentatively interpreted as evidence for the important role of dissolved oxygen species in product formation.[15] To confirm the non-reversible character of the activation period, in particular for Ag nanoparticles, an increasing/decreasing/increasing temperature testing protocol should lead to different catalytic performances in terms of activity and S(EO) for Ag5/SiO$_2$–N$_2$. Figure S9a shows the results of the applied program. Within the first increasing branch of the temperature the development of the S(EO) is distinctly visible, starting at 150 °C with around 20 % and finally reaching 58 %. The second increasing branch (ca. 25 to 35 h TOS) shows only minor changes in terms of S(EO) (58 to 62 %) as a function of the temperature, but significantly higher formation rates for EO than CO$_2$. Since 170 °C was selected three times as a reaction temperature, Figure S9b highlights the changes as a function of time. The continuously decreasing CO$_2$ formation rates and stable EO formation rates lead to an increased S(EO). This serves as (another) experimental evidence that activation means non-reversible consumption of unselective oxygen species towards a selective, oxygen poor state of Ag. Due to the insulating character of supported Ag particles and the oxygen of the supports (SiO$_2$, $\alpha$-Al$_2$O$_3$), a discrimination in electrophilic or nucleophilic oxygen species was not possible. However, based on the discussed oxygen poor character of the Ag particles in the selective state, the concentration of atomic oxygen species on the surface and its stability seems to be critical. To elucidate if any oxygen, stored in/on Ag, is needed at all to activate the reactants, microcalorimetry is applied (Figure 7). Prior to a surface titration at 230 °C with C$_2$H$_4$ and O$_2$, the oxygen in/on the supported Ag catalysts is removed under H$_2$ atmosphere at 400 °C ("chemically cleaned"). Subsequent dosing of C$_2$H$_4$ showed no measureable $\Delta H_{ads}$ (differential heat of adsorption). Adding O$_2$ resulted in $\Delta H_{ads}$ values between 55 kJ·mol$^{-1}$ (Ag5/
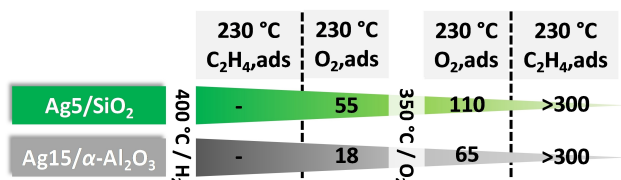
**Figure 7.** Microcalorimetry study of Ag5/SiO$_2$ and Ag15/$\alpha$-Al$_2$O$_3$ to probe the ability in activating O$_2$ and C$_2$H$_4$ at 230°C after different pretreatment conditions (400°C in H$_2$ and 350°C in O$_2$). The initial differential heat of adsorption values are given in kJ·mol$^{-1}$.

SiO$_2$) and 18 kJ·mol$^{-1}$ (Ag15/$\alpha$-Al$_2$O$_3$), still in the range where molecularly adsorbed O$_2$ is adsorbed.[19] In an attempt to dissolve/store again traces of oxygen in/on Ag, both samples were treated in O$_2$ at 350°C (above the Tamman temperature of Ag). Dosing again O$_2$ leads to significantly increased $\Delta H_{ads}$ of 110 kJ·mol$^{-1}$ (Ag5/SiO$_2$) and 65 kJ·mol$^{-1}$ (Ag15/$\alpha$-Al$_2$O$_3$), in the range where O$_2$ is activated dissociatively.[19] This is interpreted as a successful incorporation of oxygen in/on Ag by high temperature activation (350°C) as responsible for the O$_2$ activation at reaction conditions. The $\Delta H_{ads}$ for Ag nanoparticles is increased following its stronger Ag–O interaction, interpreted as PS dependent oxophilicity. When titrating with C$_2$H$_4$ again, an enormous heat evolution due to a chemical reaction with the stored atomic oxygen is observed ($>$300 kJ·mol$^{-1}$). Obviously, a small quantity of dissolved oxygen appears to be enough to activate[24,36a] O$_2$ and to form Ag$^{\delta+}$O$_x$ to facilitate ethylene adsorption/reaction.[42] As a consequence, purely metallic Ag$^0$ (without Ag $d$-/O $p$-hybridized states, "closed $d$-band")[43] is unable to activate the reactants.[34b] In turn, the oxygen traces needed for an active Ag$^{\delta+}$O$_x$ are within the detection limit/resolution of the TDS setup.[35d] Under the assumption that the surface sites quantified by ethylene adsorption (30.8 μmol/g$_{cat}$)[19] and the quantified atomic oxygen amount desorbing in region I (Figure 4a, 14.64 μmol/g$_{cat}$) is solely present on the surface, a coverage in the range of 0.5

monolayers (ML) is estimated. In the context of the almost absent oxygen desorption signal after reaching a selective state (Figure 6), the surface coverage is in the range of $<$0.005 ML ($<$1% of the starting value, 0.07 μmol/g$_{cat}$).

**Kinetic Evaluation**

Based on the discussed catalytic investigation a kinetic analysis with respect to Arrhenius plots and corresponding apparent activation energies ($E_A$) of EO and CO$_2$ formation was conducted (Figure 8). Figure 8(a) shows the $E_A$ of Ag5/SiO$_2$ and Ag15/$\alpha$-Al$_2$O$_3$ after reaching steady state (Figure S4, 30–60 h TOS; Figure S9, 25–35 h TOS). The $E_A$ for EO are very similar (Ag15/$\alpha$-Al$_2$O$_3$: 98$\pm$1 kJ·mol$^{-1}$ and Ag5/SiO$_2$: 96$\pm$1 kJ·mol$^{-1}$) evidencing that the nature of the active Ag and the formation mechanism is identical independent of the Ag PS. The $E_A$ for CO$_2$ of the reference system is slightly higher than for the Ag nanoparticles (Ag15/$\alpha$-Al$_2$O$_3$: 114$\pm$3 kJ·mol$^{-1}$ and Ag5/SiO$_2$: 103$\pm$5 kJ·mol$^{-1}$), which might explain the lower S(EO) reasoned in the stronger Ag–O interaction leading locally to an unwanted oxygen enrichment. This interpretation is supported by Figure 8(b) showing the $E_A$ of Ag5/SiO$_2$–N$_2$ during and after the activation period. The $E_A$ for EO is identical to the values obtained from the activated sample (98$\pm$2 kJ·mol$^{-1}$). The $E_A$ for CO$_2$ is different for the activation phase (48$\pm$4 kJ·mol$^{-1}$) and the activated sample (100$\pm$2 kJ·mol$^{-1}$) extracted from two linear fits. This means, in the low temperature regime (160–180°C) when the sample is still rich in oxygen and unselective, the $E_A$ for CO$_2$ is significantly decreased and in the high temperature regime close to the steady state values (180–200°C) almost doubled. Since the ln(rate) of the EO formation follows during the entire temperature range a linear behavior, the unselective sites are removed during activation without their transformation into selective ones (Figure S5). As a consequence, ethylene adsorbing on an oxygen enriched surface reacts unselectively to CO$_2$ (or to acetaldehyde and then CO$_2$) but on a surface poor in oxygen not necessarily to EO. This
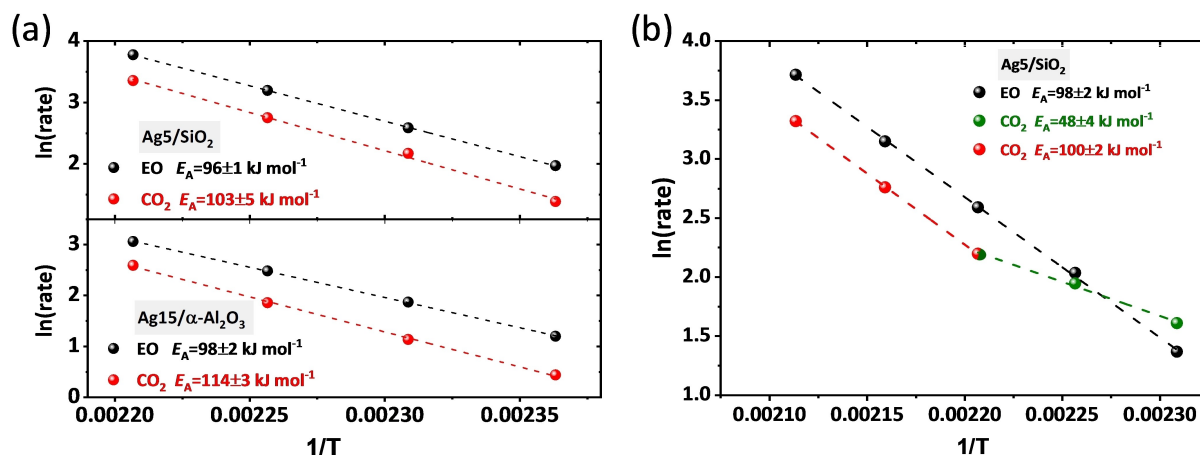


**Figure 8.** Arrhenius plots and the resulting apparent activation energies ($E_A$) for EO and CO$_2$ formation on catalysts Ag5/SiO$_2$ and Ag15/$\alpha$-Al$_2$O$_3$ after reaching steady state (a). Arrhenius plots and the resulting $E_A$ for EO and CO$_2$ formation of Ag5/SiO$_2$–N$_2$ during the activation phase and afterwards (b).

**ChemCatChem**

Full Papers
doi.org/10.1002/cctc.202000035

**Chemistry Europe**
European Chemical
Societies Publishing

evidences that different oxygen species are involved. Further, the selective transfer of an oxygen atom is part of the rate determining step. If the selective oxygen stems from an unreconstructed Ag surface, the sub-surface regime or is part of a $SO_x$ intermediate is beyond the scope of this study. However, calculating the turn over frequency (TOF, based on the ethylene adsorption capacities[19]) for both catalysts in the selective regime at almost identical $X(O_2)$ (Ag5/SiO$_2$–N$_2$ at 190 °C: $X(O_2)=$ 11.80 and for Ag15/$\alpha$-Al$_2$O$_3$ at 170 °C: $X(O_2)=$ 11.54, see also Figure 3), the TOF for Ag15/$\alpha$-Al$_2$O$_3$ is almost three-times higher compared to Ag5/SiO$_2$ (for the EO and CO$_2$ formation, see Figure S10). In light of the oxygen poor Ag surfaces in the selective state, these results might be explained by different strength of the Ag–O interaction leading to a decreased TOFs for the Ag nanoparticles independent of the reaction path (EO or CO$_2$ formation). This is generally named as particle size effect.

## A DFT perspective

At first glance this need for low atomic oxygen concentration is at odds with older proposals suggesting surface oxides are needed for EO production.[16,36a,44] The reasons for the requirement of low atomic oxygen concentration can, however, be seen when considering how it reacts with adsorbed ethylene as a function of oxygen coverage. To do so it is helpful to begin by examining the high coverage limit of oxygen. The reaction between ethylene and atomic oxygen is often thought to proceed through an oxometallacycle (OMC) intermediate,[35a,44b] where the OC$_2$H$_4$ fragment is bound to the surface through an Ag–O and an Ag–C bond (Figure S11). In the OMC mechanism ethylene reacts with O to form an OMC, which then decomposes into EO or AcH (acetaldehyde). As AcH rapidly burns on Ag surfaces, the branching ratio to the two products places an upper limit on EO selectivity. On the bulk oxide surface the OMC mechanism is predicted to appear once surface O vacancies are present, and is predicted to favor AcH production by 31 kJ·mol$^{-1}$,[44b] making oxygen on the reduced oxide surface selective to AcH, and hence CO$_2$, through the OMC mechanism. Similar behavior has been seen on the oxygen induced surface reconstructions (nucleophilic oxygen) that can form at the oxygen chemical potentials relevant for ethylene epoxidation.[34b,35b,c] In particular, both the oxygen reconstructed Ag(110)[34] and Ag(111)[34b] surfaces are found to selectively produce AcH/CO$_2$. Thus, the (nucleophilic) oxygen concentration should be minimized to achieve high $S$(EO). On unreconstructed surfaces, adsorbed oxygen cab form EO at a comparable rate to AcH.[44b] Such a phase is also pertinent to catalysis; a low coverage of oxygen has been observed on unreconstructed Ag surfaces, again, at oxygen chemical potentials relevant for ethylene epoxidation.[35c,d] The unreconstructed atomic oxygen phase also likely plays a role in mediating the coverage of electrophilic oxygen during catalysis.[34b] Thus, it is critical to understand how atomic oxygen on the surface should be managed to achieve high $S$(EO). How the chemistry of this phase changes as a function of coverage is, however, unclear. To investigate the role of oxygen coverage on the OMC

branching ratio we performed a series a DFT calculations including the exchange-hole dipole moment model for dispersion.[23] Here we examined OMC formation and its subsequent decomposition into AcH/EO using a (3×3) surface unit cell of Ag(111) with 1–4 oxygen adatoms on the surface, 1/9–4/9 mononlayer coverage (ML). (For completeness a (4×4) cell with 2/16 ML oxygen was also included.) The lower coverage range is near that observed on Ag surfaces,[35c,d] while the higher coverage is in the range of the maximum oxygen coverage seen in this work (~0.5 ML). In addition, kinetic Monte-Carlo modelling on the surface coverage of oxygen on Ag (111) identified a pressure dependent phase with a low coverage of oxygen < 0.05 ML.[45] Figure 9 shows the activation energies to EO and AcH computed on these surfaces plotted as a function of the corresponding heats of reaction. The stability of the OMC intermediate is interpreted as descriptor for selectivity towards EO.[46] Inspection of Figure 9 reveals the Bell-Evans-Polanyi principle holds for the OMC decomposition; the activation energy scales with the heat of reaction. Moreover, the activation energies also scale with the coverage of adsorbed oxygen, with the low coverage cases having nearly equivalent activation energies to EO and AcH. Conversely, at 4/9 ML oxygen coverage, approximately the maximum seen in this work, the activation energy to AcH is 15 kJ·mol$^{-1}$ below that to EO. This finding shows that, regardless of its nature, adsorbed atomic oxygen tends to favor AcH/CO$_2$ production at high oxygen coverage. This behavior can be rationalized by considering that the branching ratio in the OMC mechanism is mediated by the relative strength of its C–Ag and O–Ag bonds, with decomposition to EO favored by an increase in O–Ag bond strength relative to C–Ag.[47] Increasing the surface oxygen coverage will increase the amount of Ag$^{\delta+}$ and O adatom repulsion,[43b] which will favor AcH production. This repulsive behavior is directly evidenced for the Ag5/SiO$_2$ nanoparticles by the TDS $^{18}O_2$ exchange experiments. In short, the activation barriers calculated for the formation of EO vs. AcH as function
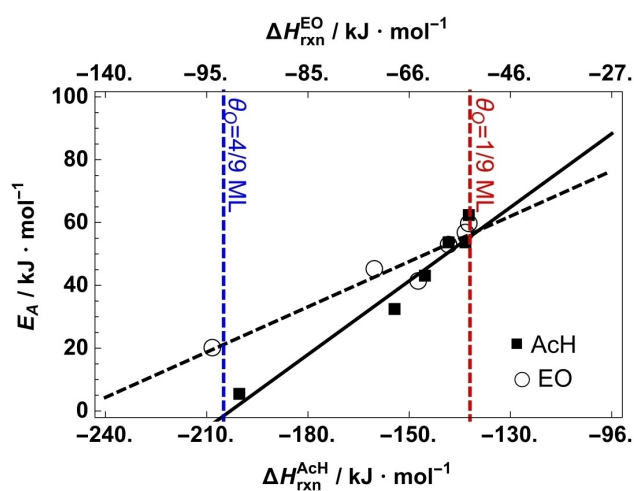


**Figure 9.** DFT calculations of the activation barriers for the formation of EO and AcH from an OMC intermediate as a function of the oxygen coverage on Ag (111).

**ChemCatChem**

**Full Papers**
doi.org/10.1002/cctc.202000035

**Chemistry**
**Europe**
European Chemical
Societies Publishing

of the oxygen coverage on the Ag surface gives a direct explanation for the experimental findings: increasing the concentration of atomic oxygen adsorbed on Ag reduces EO selectivity (Figure 3, 6 and 7) regardless of whether it is present in an unreconstructed adatom phase or as nucleophilic oxygen.

## Conclusion

Based on the advanced synthesis of supported Ag nanoparticles <6 nm with a narrow size distribution (Ag5/SiO$_2$ model catalysts),[19] we demonstrate its activity and selectivity in the ethylene epoxidation under industrially relevant conditions. The high strength of the Ag–O interaction allowed a resolution of the activation period and the identification of the selective state of Ag. The concept of an oxygen poor and selective state of Ag is independent of the Ag particle size and transferable to a Ag15/$\alpha$-Al$_2$O$_3$ reference system. Complementary TDS experiments of Ag5/SiO$_2$ and Ag15/$\alpha$-Al$_2$O$_3$ extracted the differences in Ag–O interaction also with respect to quantity and accessibility. The Ag nanoparticles exhibit a high strength in Ag–O interaction, coupled to a comparably high oxygen concentration and low accessibility. These findings make the transformation of Ag nanoparticles into a selective catalyst challenging and serve as explanation on the diverse performances discussed in the literature. The present findings correlate well with a suite of spectroscopic studies aimed at finding the oxygen species responsible for selective oxidation. The standard picture on the roles of nucleophilic (combustion) and electrophilic[48] (selective) oxygen is oversimplified, since under reaction conditions nucleophilic oxygen does not appear to be necessary. Adsorbed atomic oxygen, as shown by isotope exchange experiments, can easily migrate into the sub-surface region[49] where it can modify the electronic structure of Ag. As a consequence, a key to a selective state of the catalyst is to minimize the atomic oxygen on the surface. In industrially applied systems this is realized by promoters.[50] Due to the strong Ag–O interaction of nanoparticles (higher oxophilicity), not only the activation phase is intriguing, but also the oxygen poor Ag surface might accumulate locally an excess of adsorbed oxygen leading to a lowered $S$(EO) and $E_A$ of CO$_2$. Further, the TOFs for the EO and CO$_2$ formation of the Ag nanoparticles are negatively affected (~1/3 compared to Ag15/$\alpha$-Al$_2$O$_3$) and a distinct PS effect is evidenced.

In summary, the concept of highly dispersed nanoparticles creating more active sites is, particularly for Ag, however, not without pitfalls. The design challenge remains in the transformation of reactive sites into selective ones. The present case illustrates how the reaction of nanostructures with unexpected stability parameters may override the positive effect of higher dispersion. The intriguing Ag–O chemistry in combination with a PS dependent activation led to the controversially discussed role of Ag nanoparticles and a PS effect, which has now been understood and clarified.

## Supporting Information

Additional information on the PS distribution, kinetic analysis and DFT calculations are given.

## *Conflict of Interest*

The authors declare no conflict of interest.

**Keywords:** Ag–O interaction · Ag nanoparticles · ethylene epoxidation · oxophilicity · supported Ag catalysts · selective state

[1] R. Schlögl, *Angew. Chem. Int. Ed.* **2015**, *54*, 3465–3520.
[2] a) R. Schlögl, S. B. Abd Hamid, *Angew. Chem. Int. Ed.* **2004**, *43*, 1628–1637; b) J. R. Anderson, *Sci. Prog.* **1985**, *69*, 461–484.
[3] J. P. den Breejen, P. B. Radstake, G. L. Bezemer, J. H. Bitter, V. Frøseth, A. Holmen, K. P. d Jong, *J. Am. Chem. Soc.* **2009**, *131*, 7197–7203.
[4] A. Ueno, H. Suzuki, Y. Kotera, *J. Chem. Soc. Faraday Trans. 1* **1983**, *79*, 127–136.
[5] J. Hoffmann, I. Meusel, J. Hartmann, J. Libuda, H. J. Freund, *J. Catal.* **2001**, *204*, 378–392.
[6] N. I. Jaeger, A. L. Jourdan, G. Schulz-Ekloff, *J. Chem. Soc. Faraday Trans.* **1991**, *87*, 1251–1257.
[7] I. Kasatkin, P. Kurr, B. Kniep, A. Trunschke, R. Schlögl, *Angew. Chem. Int. Ed.* **2007**, *46*, 7324–7327.
[8] Y. Lei, F. Mehmood, S. Lee, J. Greeley, B. Lee, S. Seifert, R. E. Winans, J. W. Elam, R. J. Meyer, P. C. Redfern, D. Teschner, R. Schlögl, M. J. Pellin, L. A. Curtiss, S. Vajda, *Science* **2010**, *328*, 224–228.
[9] J. T. Miller, A. J. Kropf, Y. Zha, J. R. Regalbuto, L. Delannoy, C. Louis, E. Bus, J. A. van Bokhoven, *J. Catal.* **2006**, *240*, 222–234.
[10] a) J. E. van den Reijen, S. Kanungo, T. A. J. Welling, M. Versluijs-Helder, T. A. Nijhuis, K. P. de Jong, P. E. de Jongh, *J. Catal.* **2017**, *356*, 65–74; b) J. C. Wu, P. Harriott, *J. Catal.* **1975**, *39*, 395–402.
[11] X. E. Verykios, F. P. Stein, R. W. Coughlin, *J. Catal.* **1980**, *66*, 368–382.
[12] S. Cheng, A. Clearfield, *J. Catal.* **1985**, *94*, 455–467.
[13] J. K. Lee, X. E. Verykios, R. Pitchai, *Appl. Catal.* **1989**, *50*, 171–188.
[14] S. N. Goncharova, E. A. Paukshtis, B. S. Bal'zhinimaev, *Appl. Catal. A* **1995**, *126*, 67–84.
[15] A. J. F. van Hoof, E. A. R. Hermans, A. P. van Bavel, H. Friedrich, E. J. M. Hensen, *ACS Catal.* **2019**, *9*, 9829–9839.
[16] D. V. Demidov, I. P. Prosvirin, A. M. Sorokin, T. Rocha, A. Knop-Gericke, V. I. Bukhtiyarov, *Kinet. Catal.* **2011**, *52*, 855–861.
[17] A. P. Fotopoulos, K. S. Triantafyllidis, *Catal. Today* **2007**, *127*, 148–156.
[18] a) M. Boudart, *Adv. Catal.* **1969**, *20*, 153; b) R. van Hardeveld, F. Hartog, *Adv. Catal.* **1972**, *22*, 75–113; c) C. T. Campbell, J. R. V. Sellers, *Faraday Discuss.* **2013**, *162*, 9–30; d) C. T. Campbell, Z. Mao, *ACS Catal.* **2017**, *7*, 8460–8466.
[19] M. Lamoth, M. Plodinec, L. Scharfenberg, S. Wrabetz, F. Girgsdies, T. Jones, F. Rosowski, R. Horn, R. Schlögl, E. Frei, *ACS Appl. Nano Mater.* **2019**, *2*, 2909–2920.
[20] T. Rosendahl, T. Mäurer, C. K. Dobner, A. Lehr, J. Wanka, BASF SE, Ludwigshafen (GER), Germany, **2013**, p. 55.
[21] A. Coelho, *TOPAS: General Profile and Structure Analysis Software for Powder Diffraction Data;* Bruker AXS GmbH: Karlsruhe, Germany **2014**, version 5.

[22] P. Giannozzi, S. Baroni, N. Bonini, M. Calandra, R. Car, C. Cavazzoni, D. Ceresoli, G. L. Chiarotti, M. Cococcioni, I. Dabo, A. Dal Corso, S. de Gironcoli, S. Fabris, G. Fratesi, R. Gebauer, U. Gerstmann, C. Gougoussis, A. Kokalj, M. Lazzeri, L. Martin-Samos, N. Marzari, F. Mauri, R. Mazzarello, S. Paolini, A. Pasquarello, L. Paulatto, C. Sbraccia, S. Scandolo, G. Sclauzero, A. P. Seitsonen, A. Smogunov, P. Umari, R. M. Wentzcovitch, *J. Phys. Condens. Matter* **2009**, *21*, 395502.

[23] a) A. D. Becke, E. R. Johnson, *J. Chem. Phys.* **2007**, *127*, 154108; b) A. Otero-de-la-Roza, E. R. Johnson, *J. Chem. Phys.* **2012**, *136*, 174109.

[24] T. E. Jones, R. Wyrwich, S. Böcklein, E. A. Carbonio, M. T. Greiner, A. Y. Klyushin, W. Moritz, A. Locatelli, T. O. Menteş, M. Á. Niño, A. Knop-Gericke, R. Schlögl, S. Günther, J. Wintterlin, S. Piccinin, *ACS Catal.* **2018**, *8*, 3844–3852.

[25] A. Dal Corso, *Comput. Mater. Sci.* **2014**, *95*, 337–350.

[26] N. Marzari, D. Vanderbilt, A. De Vita, M. C. Payne, *Phys. Rev. Lett.* **1999**, *82*, 3296–3299.

[27] E. R. Jette, F. Foote, *J. Chem. Phys.* **1935**, *3*, 605–616.

[28] N. Koga, S. Yamada, T. Kimura, *J. Phys. Chem. C* **2013**, *117*, 326–336.

[29] W. M. Haynes, *CRC Handbook of Chemistry and Physics, 96th Edition*, CRC Press, **2015**.

[30] W. Luo, W. Hu, S. Xiao, *J. Phys. Chem. C* **2008**, *112*, 2359–2369.

[31] R. W. Clayton, S. V. Norval, in *Catalysis: Volume 3, Vol. 3* (Eds.: C. Kemball, D. A. Dowden), The Royal Society of Chemistry, **1980**, pp. 70–97.

[32] a) J. M. Kanervo, T. J. Keskitalo, R. I. Slioor, A. O. I. Krause, *J. Catal.* **2006**, *238*, 382–393; b) G. W. Busser, O. Hinrichsen, M. Muhler, *Catal. Lett.* **2002**, *79*, 49–54.

[33] a) M. Bowker, M. A. Barteau, R. J. Madix, *Surf. Sci.* **1980**, *92*, 528–548; b) X. Bao, J. Deng, S. H. Dong, *Surf. Sci.* **1985**, *163*, 444–456; c) G. Rovida, *J. Phys. Chem.* **1976**, *80*, 150–154.

[34] a) C. T. Campbell, M. T. Paffett, *Surf. Sci.* **1984**, *139*, 396–416; b) T. E. Jones, R. Wyrwich, S. Böcklein, T. C. R. Rocha, E. A. Carbonio, A. Knop-Gericke, R. Schlögl, S. Günther, J. Wintterlin, S. Piccinin, *J. Phys. Chem. C* **2016**, *120*, 28630–28638.

[35] a) S. Linic, M. A. Barteau, *J. Am. Chem. Soc.* **2002**, *124*, 310–317; b) W.-X. Li, C. Stampfl, M. Scheffler, *Phys. Rev. B* **2003**, *68*, 165412; c) T. E. Jones, T. C. R. Rocha, A. Knop-Gericke, C. Stampfl, R. Schlögl, S. Piccinin, *Phys. Chem. Chem. Phys.* **2015**, *17*, 9288–9312; d) E. A. Carbonio, T. C. R. Rocha, A. Y. Klyushin, I. Píš, E. Magnano, S. Nappini, S. Piccinin, A. Knop-Gericke, R. Schlögl, T. E. Jones, *Chem. Sci.* **2018**, *9*, 990–998.

[36] a) V. I. Bukhtiyarov, I. P. Prosvirin, R. I. Kvon, *Surf. Sci.* **1994**, *320*, L47-L50; b) R. Wyrwich, T. E. Jones, S. Günther, W. Moritz, M. Ehrensperger, S. Böcklein, P. Zeller, A. Lünser, A. Locatelli, T. O. Menteş, M. Á. Niño, A. Knop-Gericke, R. Schlögl, S. Piccinin, J. Wintterlin, *J. Phys. Chem. C* **2018**, *122*, 26998–27004.

[37] L. K. Ono, B. R. Cuenya, *J. Phys. Chem. C* **2008**, *112*, 18543–18550.

[38] S. Böcklein, S. Günther, J. Wintterlin, *Angew. Chem. Int. Ed.* **2013**, *52*, 5518–5521.

[39] a) C. T. Campbell, *Surf. Sci.* **1985**, *157*, 43–60; b) C. T. Campbell, M. T. Paffett, *Surf. Sci.* **1984**, *143*, 517–535.

[40] X.-C. Guo, R. J. Madix, *J. Phys. Chem. B* **2001**, *105*, 3878–3885.

[41] I. E. Wachs, S. R. Kelemen, *J. Catal.* **1981**, *71*, 78–87.

[42] T. E. Jones, T. C. R. Rocha, A. Knop-Gericke, C. Stampfl, R. Schlögl, S. Piccinin, *ACS Catal.* **2015**, *5*, 5846–5850.

[43] a) L. Zwiener, T. Jones, E. H. Wolf, F. Girgsdies, M. Plodinec, A. Y. Klyushin, E. Willinger, F. Rosowski, R. Schlögl, E. Frei, *Eur. J. Inorg. Chem.* **2019**, *2019*, 2333–2345; b) W.-X. Li, C. Stampfl, M. Scheffler, *Phys. Rev. B* **2002**, *65*, 075407.

[44] a) C. Stegelmann, N. C. Schiødt, C. T. Campbell, P. Stoltze, *J. Catal.* **2004**, *221*, 630–649; b) M. O. Özbek, R. A. van Santen, *Catal. Lett.* **2013**, *143*, 131–141.

[45] M. Huš, M. Grilc, A. Pavlišič, B. Likozar, A. Hellman, *Catal. Today* **2019**, *338*, 128–140.

[46] L. Zhu, W. Zhang, J. Zhu, D. Cheng, *Appl. Catal. A* **2017**, *538*, 27–36.

[47] A. Kokalj, P. Gava, S. de Gironcoli, S. Baroni, *J. Catal.* **2008**, *254*, 304–309.

[48] T. C. R. Rocha, A. Oestereich, D. V. Demidov, M. Hävecker, S. Zafeiratos, G. Weinberg, V. I. Bukhtiyarov, A. Knop-Gericke, R. Schlögl, *Phys. Chem. Chem. Phys.* **2012**, *14*, 4554–4564.

[49] T. E. Jones, T. C. R. Rocha, A. Knop-Gericke, C. Stampfl, R. Schlögl, S. Piccinin, *Phys. Chem. Chem. Phys.* **2014**, *16*, 9002–9014.

[50] C.-J. Chen, J. W. Harris, A. Bhan, *Chem. Eur. J.* **2018**, *24*, 12405–12415.